

Producing $\mu\text{Bq}/\text{m}^3$ level low ^{226}Ra ultrapure water for the Jiangmen Underground Neutrino Observatory

Authors: Xu, Xiting, Dr. Cong Guo, Liu, Prof. Jinchang, Dr. Yongpeng Zhang, Liang, Dr. Xiaohua, WEN, Xin-Jian, Professor Changgen Yang, TANG, Prof. Quan, Lv, Mrs. Lidan, Niu Yuanhao, Xiao, Bin, Guo, Dr. Cong

Date: 2025-10-03T00:00:00+00:00

Abstract

The Jiangmen Underground Neutrino Observatory (JUNO), a 20~ktons low-background Liquid Scintillator detector (LS), was primarily designed to determine the neutrino mass ordering. JUNO requires UltraPure Water (UPW) with a ^{226}Ra concentration $\leq 50 \text{ Bq}/\text{m}^3$ due to the direct liquid-liquid contact between Liquid Scintillator (LS) and UPW during detector filling. To meet this stringent requirement, a highly sensitive measurement system capable of detecting $3.9\text{--}\mu\text{Bq}/\text{m}^3$ of ^{226}Ra was developed, and the 100 t/h UPW production process was optimized. By integrating selective ion-exchange resin with membrane separation technologies, UPW with a ^{226}Ra concentration of $\leq 4 \text{ Bq}/\text{m}^3$ was consistently produced, exceeding JUNO's specifications and setting a world-leading benchmark. This paper describes the design and implementation of JUNO's UPW system and the highly sensitive ^{226}Ra measurement system, along with a systematic evaluation of ^{226}Ra removal efficiency across purification stages and final water quality validation.

Full Text

Preamble

Production of $\mu\text{Bq}/\text{m}^3$ Level Low- ^{226}Ra Ultrapure Water for the Jiangmen Underground Neutrino Observatory

Xi-Ting Xu¹, Cong Guo^{2,3,4,†}, Jin-Chang Liu^{2,3,4}, Yong-Peng Zhang^{2,3,4}, Xiaohua Liang⁵, Xin-Jian Wen^{1,‡}, Chang-Gen Yang^{2,3,4}, Quan Tang^{6,§}, Li-Dan Lv⁶, Yuan-Hao Niu¹, and Bin Xiao⁷

¹Institute of Theoretical Physics, Shanxi University, Taiyuan, 030006, China

²Experimental Physics Division, Institute of High Energy Physics, Chinese Academy of Sciences, Beijing, 100049, China

³School of Physics, University of Chinese Academy of Sciences, Beijing, 100049, China

⁴State Key Laboratory of Particle Detection and Electronics, Beijing, 100049, China

⁵Astro-particle Physics Division, Institute of High Energy Physics, Chinese Academy of Sciences, Beijing, 100049, China

⁶School of Nuclear Science and Technology, University of South China, Hengyang, 421001, China

⁷School of Mechanics and Optoelectronic Physics, Anhui University of Science and Technology, Huainan, 232001, China

The Jiangmen Underground Neutrino Observatory (JUNO), a 20-kiloton low-background liquid scintillator detector, was primarily designed to determine the neutrino mass ordering. JUNO requires ultrapure water (UPW) with a ^{226}Ra concentration below $50\ \mu\text{Bq}/\text{m}^3$ due to direct liquid-liquid contact between the liquid scintillator (LS) and UPW during detector filling. To meet this stringent requirement, a highly sensitive measurement system capable of detecting $3.9\ \mu\text{Bq}/\text{m}^3$ of ^{226}Ra was developed, and the 100 t/h UPW production process was optimized. By integrating selective ion-exchange resin with membrane separation technologies, UPW with a ^{226}Ra concentration of less than $4\ \mu\text{Bq}/\text{m}^3$ was consistently produced, exceeding JUNO's specifications and establishing a world-leading benchmark. This paper describes the design and implementation of JUNO's UPW system and the highly sensitive ^{226}Ra measurement system, along with a systematic evaluation of ^{226}Ra removal efficiency across purification stages and final water quality validation.

Keywords: JUNO, ultrapure water, ^{226}Ra , reverse osmosis, resin

Introduction

The Jiangmen Underground Neutrino Observatory (JUNO) [1, 2] is a multi-purpose experiment designed primarily to determine the neutrino mass ordering and precisely measure neutrino oscillation parameters by detecting reactor antineutrinos. With 20 kilotons of low-background liquid scintillator and an unprecedented energy resolution of 3% at 1 MeV, JUNO represents the largest liquid-scintillator-based underground neutrino observatory, capable of addressing numerous important topics in astroparticle physics. JUNO's extensive physics program encompasses supernova neutrinos, atmospheric neutrinos, solar neutrinos, geoneutrinos, and searches for new physics [1, 2]. Located in an underground laboratory with 700 m of overburden, the muon flux at the JUNO site is approximately $4\ \text{mHz}/\text{m}^2$ with a mean energy of 207 GeV [3]. The primary detection channel for reactor antineutrinos in JUNO is inverse beta decay on protons, with an expected detection rate of only 60 reactor antineutrino events per day. Consequently, strict control of radioactive background is essential [4].

Figure 1 [Figure 1: see original paper] shows a schematic drawing of the JUNO detector, which comprises a central detector (CD), a water Cherenkov detector (WCD), and a top tracker (TT) detector. The CD contains 20 kilotons of ultrapure liquid scintillator within a spherical acrylic vessel and is submerged in the WCD, which contains 40 kilotons of ultrapure water and is equipped with 2400 20-inch microchannel plate photomultiplier tubes (MCP-PMTs). The WCD provides sufficient water shielding to protect the CD from surrounding radioactivity and also serves as a cosmic muon veto. For both background reduction and safety considerations, the CD and WCD must initially be filled simultaneously with UPW. Subsequently, the UPW in the CD is replaced with liquid scintillator at a production rate of 7 m³/h. During this replacement process, UPW and liquid scintillator will be in direct contact. Since this represents the final stage before detector operation, strict control of radionuclides in the water is essential to prevent UPW from contaminating the liquid scintillator. One of the most challenging tasks is controlling the ²²⁶Ra concentration in water to below 50 μBq/m³ [2].

In the field of low-background water purification and ²²⁶Ra detection, both the Sudbury Neutrino Observatory (SNO) [5] and Super-Kamiokande (Super-K) [6] experiments have achieved internationally recognized advances. SNO developed a measurement technique using manganese oxide-coated beads, achieving a ²²⁶Ra detection sensitivity of 10 μBq/m³. The initial ²²⁶Ra concentration in SNO's UPW was 50 μBq/m³, later reduced to 10-20 μBq/m³ through recirculation and purification [7]. Super-K adopted SNO's methodology and achieved a similar sensitivity of 10 μBq/m³, though with slightly higher ²²⁶Ra levels in its UPW: initially 61 ± 13 μBq/m³, decreasing to 32 ± 7 μBq/m³ after recirculation [8]. In terms of production scale, Super-K's water system capacity is 30 t/h [8], notably larger than SNO's 9 t/h system [5].

This paper is structured as follows. Section II describes the UPW system for the WCD. Section III details the highly sensitive ²²⁶Ra measurement system with a detection limit of 3.9 μBq/m³. The measurement results for ²²⁶Ra concentration after each purification stage and in the final product water are presented in Section IV. Potential upgrades to the system for enhanced ²²⁶Ra removal are discussed in Section V, and a summary of the work is provided in Section VI.

II. UPW System

The JUNO experiment employs a 100 t/h UPW system to provide 40 kilotons of UPW for the WCD. This system produces water meeting the following specifications: resistivity greater than 18.2 MΩ · cm, ²²²Rn concentration below 1×10^4 μBq/m³, and minimum temperature of 17 °C, ensuring high muon detection efficiency in the WCD, negligible radioactive contribution to the CD, and thermal stability for the CD [1]. Furthermore, for the initial filling of the acrylic vessel, this system must deliver UPW at 50 t/h with a ²²⁶Ra concentration below 50 μBq/m³ [2].

The JUNO 100 t/h UPW system utilizes tap water as feedwater to produce UPW compliant with China's national electronic grade EW-I standard [9]. As shown in Figure 2 [Figure 2: see original paper], the system comprises aboveground and underground sections. The aboveground treatment system consists of sequential units: bag filters (5 μm pore size), multi-media filters (stratified quartz sand, activated carbon, anthracite), activated carbon filters (coconut shell-derived carbon), softening resin columns (special ^{226}Ra removal resin from a Chinese manufacturer), cartridge filters (5 μm pore size), and reverse osmosis (RO) membranes.

Pretreatment begins with mechanical filtration via bag filters for bulk particulate removal, followed by multi-media filtration for suspended solids reduction. Subsequent activated carbon adsorption removes residual chlorine, organic compounds, ammonia-nitrogen species, nitrites, trace heavy metals, and microbial contaminants. Ion-exchange softening achieves $\text{Ca}^{2+}/\text{Mg}^{2+}$ removal through cationic substitution. After intermediate storage, water passes through cartridge filters (5 μm) to protect downstream equipment. The RO array provides primary desalination via semipermeable membranes, achieving near-complete ionic rejection [10].

The multi-media filters, activated carbon units, and softening resin are regenerable. Multi-media filters and activated carbon filters undergo hydraulic backwashing to restore capacity, while softening resins are regenerated with NaCl brine to displace accumulated ions and restore exchange capacity, ensuring sustainable long-term operation. Product water from the aboveground system is transferred underground through a 1,300 m stainless-steel pipeline. With an elevation differential of 450 m, water first passes through a pressure-reducing valve before entering the storage tank.

The underground water system includes secondary RO membranes (enhanced desalination), an electrodeionization (EDI) device, cartridge filters (0.1 μm pore size), total organic carbon (TOC) removal, ultraviolet (UV) sterilization, degassing membranes, a microbubble generator, heat exchangers, and ultrafiltration (UF). The secondary RO membranes provide additional ion removal. EDI units combine ion-selective membranes and resin under DC fields for continuous deionization without chemical regeneration [11]. Cartridge filters capture residual particles. TOC/UV systems sterilize through UV irradiation while oxidatively decomposing organics. Degassing membranes, employing hollow fibers, vacuum pumps, and nitrogen purging, remove dissolved gases via partial pressure differentials and are critical for ^{222}Rn removal from water [12–14]. Microbubble generators enhance the ^{222}Rn removal efficiency of degassing membranes by reloading nitrogen into water [12, 14]. Heat exchangers regulate water temperature. UF membranes (0.1 μm pore size) remove trace amounts of ions, particles, colloids, and bacteria from water.

The 100 t/h UPW system supplies water for both the WCD and the initial filling of the CD. Owing to their distinct requirements, the two streams undergo separate treatments. The CD-bound water, which contacts the liquid scintillator

directly, receives additional UF for enhanced removal of ionic contaminants ($^{238}\text{U}/^{232}\text{Th}/^{226}\text{Ra}$). The WCD-bound water, however, is routed through a dedicated heat exchanger to remove heat from the submerged PMT electronics, thereby ensuring stable detector temperatures.

III. ^{226}Ra Concentration in Water Measurement

The required ^{226}Ra concentration of $50 \mu\text{Bq}/\text{m}^3$ ($2 \times 10^{-21} \text{ g}/\text{g}$) is beyond the detection capability of conventional methods like high-purity germanium spectrometry [15] and inductively coupled plasma mass spectrometry [16]. Consequently, a custom system was developed that determines ^{226}Ra activity by measuring its gaseous daughter, ^{222}Rn .

A. Measurement Principle

The initial step in measuring ^{226}Ra concentration in water via ^{222}Rn emanation is ^{226}Ra pre-concentration. The method leverages the strong adsorption of ^{226}Ra onto MnO_2 [7, 17, 18], using laboratory-synthesized manganese fiber (Mn-fiber) [19, 20]. Following ^{226}Ra extraction, the activity of ^{222}Rn emanated from the Mn-fiber during a sealed period is measured. Figure 3 [Figure 3: see original paper] illustrates the relevant decay branch of ^{226}Ra . During sealing, the relationship between the activity of ^{226}Ra and its ^{222}Rn progeny activity can be calculated according to Eq. 1:

$$A_{Rn}(t) = A_{Ra} \times \frac{\lambda_{Rn}}{\lambda_{Rn} - \lambda_{Ra}} \times (e^{-\lambda_{Ra}t} - e^{-\lambda_{Rn}t})$$

where $A_{Rn}(t)$ is the ^{222}Rn activity at time t in mBq, A_{Ra} is the initial activity of ^{226}Ra extracted by Mn-fiber in mBq, λ_{Rn} is the decay constant of ^{222}Rn , λ_{Ra} is the decay constant of ^{226}Ra , and t is the Mn-fiber sealing time in days.

Given that the half-life of ^{226}Ra is significantly longer than that of ^{222}Rn (i.e., $\lambda_{Ra} \ll \lambda_{Rn}$), Eq. 1 can be simplified to:

$$A_{Ra} = \frac{A_{Rn}(t)}{1 - e^{-\lambda_{Rn}t}}$$

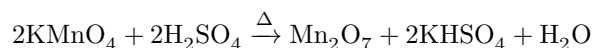
B. Measurement Procedures and Devices

The ^{226}Ra concentration measurement comprises four steps: (1) Mn-fiber synthesis, (2) ^{226}Ra extraction from water, (3) Mn-fiber encapsulation, and (4) ^{222}Rn activity determination.

1. Mn-fiber To meet JUNO' s requirement for $\mu\text{Bq}/\text{m}^3$ level ^{226}Ra measurements, we significantly reduced the ^{226}Ra background of the key adsorbent, Mn-fiber, from $17 \mu\text{Bq}/\text{g}$ to $10.7 \pm 1.5 \mu\text{Bq}/\text{g}$. This was achieved through

three major enhancements to the standard synthesis protocol [19, 20]: (1) nitric acid pre-cleaning of the polyurethane fibers, (2) moving the boiling and rinsing processes to a cleanroom, and (3) substituting distilled water with high-purity water from China Resources C' estbon Beverage (China) Co., Ltd for rinsing—the most impactful change.

The Mn-fiber is produced by creating a firm MnO_2 coating on polyurethane fibers via reaction of KMnO_4 with H_2SO_4 under heated conditions:



A photograph of the Mn-fiber is shown in Figure 4 [Figure 4: see original paper]. Gravimetric analysis indicates a 13% mass increase in polyurethane fibers after conversion to Mn-fiber.

2. Extraction Column The ^{226}Ra extraction column, illustrated in Figure 5 [Figure 5: see original paper], is constructed from an acrylic tube (20 mm inner diameter and 185 mm length) sealed with rubber gaskets and 10 mm quick-connects. The assembled unit withstands water pressures up to 5 kg/cm². Approximately 5 g of Mn-fiber is packed in the central section, flanked by polyurethane fibers at both ends to filter particulate matter. During operation, water is directed upward through the column to maximize contact with the Mn-fiber. A residential water meter (GB/T 778 compliant [21], $\pm 2\%$ accuracy) at the outlet measures the total volume of water passing through the Mn-fiber.

3. ^{222}Rn Emanation Measurement System The ^{226}Ra activity extracted by Mn-fibers was quantified by measuring its gaseous daughter ^{222}Rn using a radon emanation measurement system (Figure 6 [Figure 6: see original paper]). The system comprises a radon detector, a Mn-fiber container, a dehumidification system, a mass flow controller (MFC, Model 1179A, MKS), and a vacuum pump (Model ACP40, Pfeiffer Vacuum). All connections use metal-sealed ConFlat flanges and VCR components, ensuring leak tightness below 1×10^{-9} Pa · m³/s. Key components are summarized below, with full details described in our previous work [20].

(1) Radon Detector. The radon detector operates on the principle of electrostatic collection [22–28], where detection efficiency for radon progeny correlates with applied collection voltage and gas humidity. At 3% relative humidity and -700 V collection voltage, the detector achieves 90% collection efficiency for the ^{222}Rn progeny ^{214}Po . This corresponds to a calibration factor (CF) of 67 ± 6.7 counts per hour per Bq/m³ (cph/(Bq/m³)). The system's single-day measurement sensitivity is 0.7 mBq/m³ for ^{222}Rn [22]. For each sample measurement,

the radon detector integrates radon activity over a 24-hour data-taking period. As the measured value represents the average ^{222}Rn concentration during this interval, determination of the initial ^{222}Rn concentration requires correction for radioactive decay, calculated according to Eq. 5:

$$A_{Rn} = A_{Rn-M} \times \frac{\lambda_{Rn} \times (t_2 - t_1)}{e^{-\lambda_{Rn}t_1} - e^{-\lambda_{Rn}t_2}}$$

where A_{Rn} is the initial ^{222}Rn activity after transferring into the detector in mBq, A_{Rn-M} is the measured ^{222}Rn activity in mBq, t_1 is the start measurement time in hours, and t_2 is the end measurement time in hours.

(2) Mn-fiber Container. Two chamber types are used (Figure 7 [Figure 7: see original paper]): a standard CF35 tube (150 mm length) for 5 g samples, and a custom chamber (130 mm diameter and 300 mm length) for 300 g samples used in background measurements. All inner surfaces were electropolished to a roughness below 0.1 μm . After loading, chambers are purged with boil-off nitrogen to remove residual air and sealed for several days to allow ^{222}Rn ingrowth. The activity ratio between ^{226}Ra and ^{222}Rn can be calculated according to Eq. 2. For instance, after a 10-day sealing interval, ^{222}Rn activity reaches 83.7% of the initial ^{226}Ra activity.

(3) Dehumidification System. Mn-fibers that have extracted ^{226}Ra retain substantial water, releasing significant water vapor during radon transfer that degrades detector efficiency through humidity interference. This system comprises a liquid nitrogen tank, a solenoid valve, a dewar, a PT100 temperature sensor, and a temperature controller. Through thermostatic regulation of intermittent liquid nitrogen injection into the dewar, the system maintains $-60\text{ }^\circ\text{C}$ inside the dewar, reducing relative humidity to 3% at a 1 L/min gas flow rate without introducing background.

(4) MFC. The MFC regulates gas flow rate during radon transfer operations, with an adjustment range of 0.5-5 L/min.

(5) Vacuum Pump. Before measurements, the pump evacuates the radon detector and associated pipelines. Subsequently, boil-off nitrogen purges the emanated ^{222}Rn from the Mn-fiber container into the radon detector.

(6) Pipelines and Valves. All stainless steel gas pipelines and interconnecting valves were EP-grade components.

C. Extraction Efficiency Calibration

The efficiency of extracting ^{226}Ra from water by Mn-fiber was calibrated using a standardized ^{226}Ra solution with a concentration of $(9.04 \pm 0.53) \times 10^3\text{ }\mu\text{Bq}/\text{m}^3$. Our prior work [20] demonstrates consistent extraction efficiency across ^{226}Ra concentrations ($760\text{--}6.1 \times 10^4\text{ }\mu\text{Bq}/\text{m}^3$) and water flow rates (1.6-8 L/min). To cover ^{226}Ra concentrations from 1 to $1 \times 10^4\text{ }\mu\text{Bq}/\text{m}^3$ in JUNO, sample volumes

are varied, requiring dedicated calibration of extraction efficiency for different volumes. Rather than absolute quantification, we employed a relative scheme with volume-matched control experiments to simultaneously mitigate detector systematic uncertainties and background in this work.

Table 1 presents the calibrated ^{226}Ra extraction efficiencies across different water volumes. Throughout the test, an additional 150 μL of ^{226}Ra solution was added per 300 L of water, and the water flow rate through the Mn-fiber was maintained at 5 L/min. For water volumes below 1 m^3 passing through the Mn-fiber extraction column, ^{226}Ra extraction efficiency approached 100%. Beyond this volume, a progressive decline in ^{226}Ra adsorption efficiency was observed, likely caused by a small amount of adsorbed ^{226}Ra MnO_2 shedding.

D. Sensitivity Estimation

The sensitivity of measuring ^{226}Ra concentration in water at 95% confidence level can be estimated according to Eq. 6:

$$L = \frac{1.645 \times \sigma_{BG} \times V_s}{24 \times CF \times V_w \times \varepsilon \times 10^{-6}}$$

where L is the sensitivity in $\mu\text{Bq}/\text{m}^3$, σ_{BG} is the statistical uncertainty of the system's background event rate in counts per day (CPD), $V_s = 0.042 \text{ m}^3$ is the total volume of the measurement system, $CF = 67 \pm 6.7 \text{ cph}/(\text{Bq}/\text{m}^3)$ is the detector calibration factor, V_w is the sample water volume in m^3 , and ε is the ^{226}Ra extraction efficiency listed in Table 1. This calculation assumes a normally distributed background event rate and radioactive equilibrium between ^{222}Rn and ^{226}Ra .

The system background was determined by measuring 5 g of unused Mn-fiber following the standard sealing and analysis procedure. Ten replicate measurements yielded a mean background of 2.7 CPD (Figure 8 [Figure 8: see original paper]), reflecting contributions from both the apparatus and the Mn-fiber. Using the parameters above and Eq. 6, a sensitivity of 3.9 $\mu\text{Bq}/\text{m}^3$ for ^{226}Ra concentration in water has been derived. This calculation assumes 20 m^3 of water passes through 5 g Mn-fiber with a ^{226}Ra extraction efficiency of 89.2%, and the data-taking time for ^{222}Rn activity measurement is 24 h.

IV. Results

^{226}Ra Concentrations Across the System

Using the custom-developed device described above, the ^{226}Ra concentrations in water at different locations of the JUNO 100 t/h UPW system (marked as S1-S17 in Figure 2) were measured, with results shown in Table 2. The water volume for S1-S5 was 0.5 m^3 , for S6-S8 and S10 was 1 m^3 , for S9 and S11-S14 was 5 m^3 , and for S15-S17 was 20 m^3 . All measurements were performed after

a 10-day Mn-fiber sealing period and a 24-hour ^{222}Rn counting interval. Reported uncertainties include both statistical and systematic contributions from extraction efficiency. Sample S17 registered only 2 counts during measurement, below the mean detector background, and thus only an upper limit is provided.

In low-salinity solutions, ^{226}Ra exists predominantly as uncomplexed Ra^{2+} [29–31], making it removable via deionization processes. According to Table 2, this system reduces ^{226}Ra concentration from $4 \times 10^5 \text{ }\mu\text{Bq}/\text{m}^3$ to $<4 \text{ }\mu\text{Bq}/\text{m}^3$, representing a reduction of over five orders of magnitude. This $>99.99\%$ removal efficiency was achieved primarily through the synergistic action of softening resin and two-stage RO membranes, each exhibiting $>99\%$ ^{226}Ra removal efficiency. The ^{226}Ra removal efficiencies of the main devices in the UPW system are shown in Table 3. The slight variation in removal efficiency between the two RO stages is primarily attributable to differences in influent ^{226}Ra concentration. This system employs two polishing resins in series, with tabulated efficiency calculations assuming identical ^{226}Ra removal performance.

However, according to the data in Table 2, mechanical filtration units (e.g., filter bags, cartridges, multi-media filters) also showed incidental ^{226}Ra removal via adsorption of Ra^{2+} onto particulates, enabling co-removal during filtration. Among all devices, only RO integrates both deionization and particulate removal [32]. Additionally, the data indicate that ^{226}Ra concentration in water increased after passing through each tank, primarily attributable to air ingress through tank ventilation valves. Fiberglass-reinforced plastic tanks require pressure-equalizing vent valves to prevent structural damage during water level fluctuations. These valves introduce ambient air (unfiltered for aboveground tanks, filtered for underground tanks) containing dust-bound ^{226}Ra progenitors that solubilize upon water contact. A significant increase in ^{226}Ra concentration after the pre-treatment water tank was traced to sediment introduced during initial commissioning when sea salt was used for softening resin regeneration. Although sea salt was replaced by clean regeneration salt and the tank was flushed, residual sediment on tank walls persisted as a leaching source.

Relationship Between ^{226}Ra Concentration, Particulate Counts, and Resistivity

Table 2 also lists particulate counts and resistivity values across the water system. Particulate counts were measured using a Bettersize C400 optical particle counter (Dandong Baxter); the small sample volume (20 mL) contributed to significant data uncertainties. Resistivity was measured using an AZ8302 portable conductivity tester (Taiwan Hengxin) upstream of the secondary RO and a +GF+ Signet 9900 in-line meter downstream. Sampling measurements become unreliable when resistivity exceeds $10 \text{ M}\Omega \cdot \text{cm}$, and in-line measurements prevent modification of sampling points. These constraints resulted in missing high-resistivity data at multiple locations.

The apparent correlations between ^{226}Ra concentration, particulate counts, and

resistivity are merely a coincidental outcome of the purification process. The softening resin achieves >99% ^{226}Ra removal by ion exchange (Na^+ replaces Ra^{2+}), which minimally influences resistivity and does not filter particles due to its 100–500 μm bead size. The simultaneous decrease in all parameters is due to their collective removal through successive treatment stages.

V. Discussion

This system reduces ^{226}Ra concentration in water from $4 \times 10^5 \mu\text{Bq}/\text{m}^3$ to $4 \mu\text{Bq}/\text{m}^3$. Even though RO provides high removal efficiency for particulate matter and ions, the softening resin plays a critical complementary role. Our resin screening revealed significant variation in ^{226}Ra removal efficiency, with cationic resins demonstrating superior performance over mixed-bed (anionic/cationic) alternatives. Although the selected softening resin achieves high ^{226}Ra rejection (>99%), its pre-RO positioning is mandatory and non-interchangeable with post-RO polishing resin due to substantial organic leaching. These leachates cause measurable deterioration of water quality, primarily through resistivity reduction and TOC elevation.

Two tasks have been identified for reducing ^{226}Ra pollution sources:

(1) Thorough cleaning of the pre-treatment water tank. Periodic regeneration of softening resin, commonly performed with economical sea salt, was found to introduce sediment containing significant ^{226}Ra contamination. During the initial commissioning phase, conventional sea salt was used, resulting in a sharp increase in ^{226}Ra concentration—from $500 \mu\text{Bq}/\text{m}^3$ to $3 \times 10^5 \mu\text{Bq}/\text{m}^3$ —after water passed through the pretreatment tank. Visual inspection revealed a substantial sediment layer at the tank bottom, which subsequent analysis confirmed originated from the sea salt. The data presented in this paper were collected after switching to clean regenerant salt and performing systematic flushing. However, even after adopting clean salt and flushing, residual sediment remains adhered to tank walls, explaining the persistent increase in ^{226}Ra concentration observed after the pretreatment water tank. To fully eliminate this contamination source, thorough cleaning of the tank interior is required. As this procedure entails tank drainage and temporary system shutdown, it will be scheduled for a suitable maintenance window.

(2) Mitigation of contamination from storage tank breather valves. Storage tanks introduce measurable radiological contamination primarily through their air-admittance breather valves. Two mitigation strategies have been evaluated: installing particulate-retentive filters on breather assemblies or using boil-off nitrogen as a clean breathing gas. While nitrogen blanketing could thoroughly eliminate background contamination, it would require a dedicated gas supply system at significant cost. Furthermore, the existing boil-off nitrogen capacity at the JUNO site is insufficient to meet operational demand. Therefore, installation of filtration systems at each tank air inlet has been selected as the practical solution, which will be implemented during a

suitable maintenance period.

VI. Summary

JUNO is a multi-purpose neutrino experiment primarily designed to determine the neutrino mass ordering. To ensure detector safety and minimize background, the CD must be filled with UPW containing $<50 \mu\text{Bq}/\text{m}^3$ of ^{226}Ra before liquid scintillator introduction. A dedicated 100 t/h UPW production and circulation system was developed, integrating multi-stage purification—including specialized softening resin and reverse osmosis—with a novel, highly sensitive ($3.9 \mu\text{Bq}/\text{m}^3$) ^{226}Ra measurement system. Measurement results across purification stages demonstrated $>99\%$ ^{226}Ra removal efficiency for both the softening resin and RO. Key contamination pathways, including water tank venting and regenerant salt impurities, were identified, and corresponding mitigation strategies have been proposed.

The JUNO 100 t/h water system successfully reduced ^{226}Ra concentration from $4 \times 10^5 \mu\text{Bq}/\text{m}^3$ to $<4 \mu\text{Bq}/\text{m}^3$, achieving a reduction exceeding five orders of magnitude. This performance not only satisfies JUNO's stringent technical requirements but also represents a world-leading achievement in ultra-low- ^{226}Ra water purification.

References

- [1] F. An, G. An, Q. An et al., Neutrino physics with JUNO. *J. Phys. G* 43, 030401 (2016). <https://doi.org/10.1088/0954-3899/43/3/030401>
- [2] JUNO Collaboration, JUNO physics detector. *Prog. Part. Nucl. Phys.* (2022). <https://doi.org/10.1016/j.pnpnp.2021.103927>
- [3] C. Cao, J. Xu, M. He et al., Mass production and characterization of 3-inch PMTs for the JUNO experiment. *Nucl. Instrum. Meth. Phys. Res. Sect. A* 1005, 165347 (2021). <https://doi.org/10.1016/j.nima.2021.165347>
- [4] JUNO Collaboration, Radioactivity control strategy for the JUNO detector. *J. High Energy Phys.* 2021, 102 (2021). [http://doi.org/10.1007/JHEP11\(2021\)102](http://doi.org/10.1007/JHEP11(2021)102)
- [5] SuperK Collaboration, The Super-Kamiokande Detector. *Nucl. Instrum. Meth. Phys. Res. Sect. A* 501, 418-462 (2003). [https://doi.org/10.1016/S0168-9002\(03\)00425-X](https://doi.org/10.1016/S0168-9002(03)00425-X)
- [6] SNO Collaboration, The Sudbury Neutrino Observatory. *Nucl. Instrum. Meth. Phys. Res. Sect. A* 449, 172-207 (2000). [https://doi.org/10.1016/S0168-9002\(99\)01469-2](https://doi.org/10.1016/S0168-9002(99)01469-2)
- [7] T.C. Andersen, I. Blevis, J. Boger et al., Measurement of radium concentration in water with Mn-coated beads at the Sudbury Neutrino Observatory. *Nucl. Instrum. Meth. Phys. Res. Sect. A* 501, 399-417 (2003). [https://doi.org/10.1016/S0168-9002\(03\)00616-8](https://doi.org/10.1016/S0168-9002(03)00616-8)
- [8] T. Ueno, Radium Concentration Measurements in Super-Kamiokande Search for Magnetic Monopoles in Grand Unified Theory, Master's Thesis, University of Tokyo (2021). <https://www-sk.icrr.u-tokyo.ac.jp/assets/paper/list/pdf/mthesis/2008/master->

ueno.pdf

- [9] Electronic Grade Ultrapure Water, SJ/T 11452-2013 (2013). <https://std.samr.gov.cn/>
- [10] M. Tawalbeh, L. Qalyoubi, A. Al-Othman et al., Insights on the development of enhanced antifouling reverse osmosis membranes: Industrial applications and challenges. *Desalination* 553, 116460 (2023). <https://doi.org/10.1016/j.desal.2023.116460>
- [11] Z.U. Khan, M. Moronshing, M. Shestakova et al., Electro-deionization (EDI) technology for enhanced water treatment and desalination: A review. *Desalination* 548, 116254 (2023). <https://doi.org/10.1016/j.desal.2022.116254>
- [12] B. Wang, C. Guo, Y.G. Xie et al., Measurement of the radon concentration in the ultrapure water of JUNO-LS UPW system. *J. Instrum.* 20, P03028 (2025). <https://doi.org/10.1088/1748-0221/20/03/P03028>
- [13] Y. Nakano, T. Hokama, M. Matsubaara et al., Measurement of the radon concentration in purified water in the Super-Kamiokande IV detector. *Nucl. Instrum. Meth. Phys. Res. Sect. A* 977, 164297 (2020). <https://doi.org/10.1016/j.nima.2020.164297>
- [14] T.Y. Guan, Y.P. Zhang, B. Wang et al., Development of low-radon ultra-pure water for the Jiangmen Underground Neutrino Observatory. *Nucl. Instrum. Meth. Phys. Res. Sect. A* 1063, 169244 (2024). <https://doi.org/10.1016/j.nima.2024.169244>
- [15] G.R. Araujo, L. Baudis, Y. Biondi et al., The upgraded low-background germanium counting facility Gator for high-sensitivity γ -ray spectrometry. *J. Instrum.* 17, P08010 (2022). <https://doi.org/10.1088/1748-0221/17/08/P08010>
- [16] S. Ito, Y. Takaku, M. Ikeda et al., Determination of trace level thorium and uranium in high purity gadolinium sulfate using ICP-MS with solid-phase chromatographic extraction resins. *AIP Conf. Proc.* 1921, 030003 (2018). <https://doi.org/10.1063/1.5018990>
- [17] W.S. Moore, D.F. Reid, Extraction of radium from natural waters using manganese-impregnated acrylic fibers. *J. Geophys. Res.* 78, 8880-8886 (1973). <https://doi.org/10.1029/JC078i036p08880>
- [18] R.N. Peterson, W.C. Burnett, N. Dimova et al., Comparison of measurement methods for radium-226 on manganese-fiber. *Limnol. Oceanogr.* 7, 196-205 (2009). <https://doi.org/10.4319/lom.2009.7.196>
- [19] L.F. Xie, J.C. Liu, S.K. Qiu et al., Developing the radium measurement system for the water Cherenkov detector of the Jiangmen Underground Neutrino Observatory. *Nucl. Instrum. Meth. Phys. Res. Sect. A* 976, 164266 (2020). <https://doi.org/10.1016/j.nima.2020.164266>
- [20] C. Li, B. Wang, Y. Liu et al., Developing a $\mu\text{Bq}/\text{m}^3$ level ^{226}Ra concentration in water measurement system for the Jiangmen Underground Neutrino Observatory. *Nucl. Instrum. Meth. Phys. Res. Sect. A* 1063, 169257 (2024). <https://doi.org/10.1016/j.nima.2024.169257>
- [21] China National Standards Full-Text Disclosure System. <https://openstd.samr.gov.cn>
- [22] J.X. Wang, T.C. Andersen, J.J. Simpson, An electrostatic radon detector designed for water radioactivity measurements. *Nucl. Instrum. Meth. Phys. Res. Sect. A* 421, 601-609 (1999). [https://doi.org/10.1016/S0168-9002\(98\)01230-3](https://doi.org/10.1016/S0168-9002(98)01230-3)

- [23] Y.Y. Chen, Y.P. Zhang, Y. Liu et al., A study on the radon removal performance of low background activated carbon. *J. Instrum.* 17, P02003 (2022). <https://doi.org/10.1088/1748-0221/17/02/P02003>
- [24] C. Guo, J.C. Liu, Y.P. Zhang et al., Study on the radon removal for the water system of Jiangmen Underground Neutrino Observatory. *Radiat. Detect. Technol. Methods* 2, 48 (2018). <https://doi.org/10.1007/s41605-018-0077-8>
- [25] Y. Liu, Y.P. Zhang, J.C. Liu et al., System upgrade for $\mu\text{Bq}/\text{m}^3$ level ^{222}Rn concentration measurement. *J. Instrum.* 18, T03002 (2023). <https://doi.org/10.1088/1748-0221/18/03/T03002>
- [26] C. Li, Y. Zhang, L. Lv et al., Study on the radon adsorption capability of low-background activated carbon. *J. Radioanal. Nucl. Chem.* 333, 337-346 (2024). <https://doi.org/10.1007/s10967-023-09211-w>
- [27] Y. Nakano, H. Sekiya, S. Tasaka et al., Measurement of radon concentration in super-Kamiokande's buffer gas. *Nucl. Instrum. Meth. Phys. Res. Sect. A* 867, 108-114 (2017). <https://doi.org/10.1016/j.nima.2017.04.037>
- [28] Y. Nakano, T. Hokama, M. Matsubara et al., Measurement of the radon concentration in purified water in the Super-Kamiokande IV detector. *Nucl. Instrum. Meth. Phys. Res. Sect. A* 977, 164297 (2020). <https://doi.org/10.1016/j.nima.2020.164297>
- [29] B.L. Dickson, Radium behavior in the environment. IAEA. Vol. 1, No. 1 (1990). <https://inis.iaea.org/records/swprd-wbq70>
- [30] D. Porcelli and P.W. Swarzenski, The behavior of U- and Th-series nuclides in groundwater. *Rev. Mineral. Geochem.* 52, 317-361 (2003). <https://doi.org/10.2113/0520317>
- [31] F. Carvalho, D. Chambers, S. Fernandes et al., The environmental behaviour of radium: Revised edition. IAEA Technical Reports Series No. 476 (2014). <http://www.iaea.org/books>
- [32] PURETEC Industrial Water, The Basics - Reverse Osmosis. <https://puretecwater.com>

Note: Figure translations are in progress. See original paper for figures.

Source: ChinaXiv – Machine translation. Verify with original.